



Fluorinated electrolyte formulations design enabling high-voltage and long-life lithium metal batteries

Yuxin Rao^a, Xue Li^a, Shangquan Zhao^a, Pengfei Liu^a, Fanglin Wu^{b,c}, Xiang Liu^a, Naigen Zhou^a, Shan Fang^{a,*}, Stefano Passerini^{b,c,d,**}

^a School of Physics and Materials Science, Nanchang University, Nanchang, Jiangxi 330031, China

^b Helmholtz Institute Ulm (HIU), Helmholtzstrasse 11, Ulm 89081, Germany

^c Karlsruhe Institute of Technology (KIT), P.O. Box 3640, Karlsruhe 76021, Germany

^d Sapienza University of Rome, Chemistry Department, Piazzale a. Moro 5, Rome 00185, Italy

ARTICLE INFO

Keywords:

Fluorinated electrolytes
Lithium bis(fluorosulfonyl)imide (LiFSI)
Lithium nitrate (LiNO₃)
Solvation structure
Lithium dendrite
Lithium metal anode

ABSTRACT

The poor compatibility of carbonate-based electrolytes with lithium metal anodes results in unstable solid electrolyte interphase, leading to lithium dendrite formation, low Coulombic efficiency, and short cycle life. To address this issue, we propose a novel fluorinated electrolyte that leverages lithium bis(fluorosulfonyl)imide (LiFSI), along with fluorinated solvents. An extremely low concentration of lithium nitrate exerts a substantial impact on the Li ion solvation structure, inducing an anions-rich solvation structure, results in an inorganic-rich electrolyte interphase layer mainly composed of Li₃N and LiF, which effectively inhibits lithium dendrite formation, enhances the interfacial stability between the electrode and electrolyte, and yields excellent cycling performance in lithium metal batteries. When coupled with a high nickel content cathode (LiNi_{0.8}Co_{0.1}Mn_{0.1}O₂), the cells exhibit impressive cycling performance with 1000 cycles at 4 C, retaining 68.6 % capacity (with charge times under 15 min). Despite the relatively low oxidation stability of Dimethoxyethane in the electrolyte, the cell demonstrates exceptional high-voltage electrochemical performance, even up to 4.5 V, the cells do not show extensive electrolyte decomposition and structural changes, preserving 79.2 % capacity retention after 300 cycles. Using 50 μm lithium foil in the cells, remarkable capacity retention of 89.5 % is achieved after 400 cycles at 1 C. This remarkable compatibility between the anode and cathode represents a significant breakthrough in enhancing the reliability and performance of lithium metal batteries.

1. Introduction

Lithium metal as a key negative material to achieve high energy density “next generation” Li secondary batteries has received much attention in recent years [1–5]. However, this highly reactive metal spontaneously reacts with the electrolyte to generate solid byproducts on the surface of the electrode, i.e., forming the solid electrolyte interphase (SEI), which is typically unstable and fragile [6]. The continuous consumption of the electrolyte during lithium plating/stripping causes the SEI to constantly restructure and thicken, leading to significant interfacial impedance increase and slow lithium-ion transport kinetics [7]. Furthermore, the unstable SEI leads to uneven lithium deposition, resulting in the formation of lithium dendrites along with the accumulation of dead lithium. The lithium dendrites may penetrate the

separator to eventually contact the positive electrode, resulting in the cell short-circuit and related safety issues [8]. Effectively suppressing lithium dendrite growth and establishing a stable and resilient electrolyte interface are the main concerns that researchers are trying to address.

The structure and composition of the SEI and cathode electrolyte interphase (CEI) are influenced by the solvation structure of lithium ions within the electrolyte. In conventional electrolytes, the strong solvation properties of the solvents result in dominant coordination of lithium ions with solvent molecules, leading to the formation of many solvent-separated ion pairs (SSIPs). These SSIPs contribute to the formation of an organic-rich SEI layer with low ionic conductivity and mechanical strength, not disabling the formation of lithium dendrites [9–11]. To establish a robust and thin inorganic interfacial layer, it is essential to

* Corresponding author.

** Corresponding author at: Helmholtz Institute Ulm (HIU), Helmholtzstrasse 11, Ulm 89081, Germany.

E-mail addresses: fangshan@ncu.edu.cn (S. Fang), stefano.passerini@kit.edu (S. Passerini).

<https://doi.org/10.1016/j.nanoen.2024.109362>

Received 27 October 2023; Received in revised form 29 January 2024; Accepted 2 February 2024

Available online 6 February 2024

2211-2855/© 2024 The Author(s). Published by Elsevier Ltd. This is an open access article under the CC BY-NC-ND license (<http://creativecommons.org/licenses/by-nc-nd/4.0/>).

increase the involvement of anions within the solvation shell, i.e., to reduce the content of SSIPs favoring contact ion pairs (CIPs) and aggregates (AGGs) [12–15]. Increasing the proportion of anions is the most common and convenient approach, such as in highly concentrated electrolytes (HCE), localized highly concentrated electrolytes (LHCE), etc. Due to the scarcity of solvents, anions are taking a leading role in the solvation shell of Li^+ , yielding to the formation of more CIPs and AGGs. In addition, weakly solvating and dissociating electrolytes (WSDE) [16] have also been proposed as a new method. In WSDE, solvents with low solvation capacity are effectively displaced by weakly dissociating lithium salt anions, resulting in the generation of large CIPs and AGGs fractions.

It is known that slight molecular modifications can have substantial implications on the physical and chemical properties of materials. Therefore, introducing functional groups in solvent molecules or distinct components may be an effective strategy for developing improved electrolyte [17]. In particular, the use of fluorinated solvents in electrolytes has shown considerable promise in mitigating several challenges commonly associated with conventional electrolytes, i.e., low compatibility with lithium metal, rapid capacity decay at high voltage and high flammability [18,19]. The substitution of specific functional groups of solvent molecules with fluorine results, due to the weak polarity and strong electronegativity of the fluorine atom, in a weakened solvation by the solvent effectively promoting the coordination between anions and lithium ions [20]. Herein, two fluorinated solvents, fluoroethylene carbonate (FEC) and methyl-2,2,2-trifluoroethyl carbonate (FEMC), were employed to develop a novel fluorinated electrolyte. Their difference in energy levels, specifically, FEMC shows higher HOMO (highest occupied molecular orbital) and LUMO (lowest unoccupied molecular orbital) than FEC, indicates the former more prone to decomposition at the cathode side and the latter more likely to decompose at the anode side [21]. By selectively decomposing at the respective electrode interfaces, FEMC and FEC may selectively contribute to the composition and stability of the SEI and CEI layers. However, electrolytes based on these solvents generally suffer from limitations in terms of ionic conductivity and viscosity, resulting in lower rate capability and short cycle life [22]. Additionally, fluoride electrolytes raise storage concerns associated with the formation of hydrofluoric acid [23,24] affecting the battery performance. To overcome these issues, the inclusion of ethylene glycol dimethyl ether (DME) and LiNO_3 has been identified as a viable solution. The addition of DME is expected to improve the ionic conductivity of the fluorinated electrolyte (Fig. S1), however, its high HOMO level and poor oxidation stability make it prone to accelerated decomposition, especially at high voltages. Interestingly, the introduction of trace amounts of LiNO_3 can significantly improve the stability of the electrolyte, as its higher HOMO and lower LUMO energy levels enable preferential oxidation and reduction, leading to the formation of passivation layers that effectively mitigates electrolyte decomposition [25]. Additionally, it allows for storage over extended periods of time without noticeable change (Fig. S2). Furthermore, the presence of DME can effectively address the poor solubility of LiNO_3 [26–28]. Therefore, the two components synergistically enhance the performance and stability of the fluorinated electrolyte.

The newly developed fluorinated electrolyte has been investigated against both positive and negative electrodes in $\text{Li}|\text{Li}$ symmetric cells and $\text{Li}|\text{NCM811}$ cells, respectively, delivering remarkable cycling stability, i.e., 500 h at 2 mA cm^{-2} for symmetric cell and up to 1000 cycle at 4 C rate for the full cell. Additionally, the $\text{Li}|\text{NCM811}$ cell achieved excellent cycling stability even upon charging up to 4.5 V (79.2 % capacity retention after 300 cycles). Finally, a high-capacity pouch cell with 1200 mAh is achieved by the developed electrolyte. The distinctive formulation and superior properties of this electrolyte position it as a potential candidate to improve the electrochemical performance of lithium metal batteries.

2. Experimental section

2.1. Preparation of the electrolytes and electrode materials

Fluoroethylene carbonate (FEC, 98 %), methyl 2,2,2-trifluoroethyl carbonate (FEMC, 98 %), lithium bis(fluorosulfonyl)imide (LiFSI >98 %), and lithium nitrate (LiNO_3 , 99 %) were purchased from Aladdin. Ethylene glycol dimethyl ether (DME) was purchased from Macklin. All materials were used as received without further purification. The electrolyte was prepared in an Ar-filled glovebox with water and oxygen content ≤ 0.01 ppm. First, the 1.0 M LiFSI in FEC:FEMC (1:1 v/v) fluorinated electrolyte was prepared including 0.5 wt% of LiNO_3 (based on the total mass of solvent and LiFSI salt). To facilitate the LiNO_3 dissolution, ethylene glycol dimethyl ether (DME) was also introduced, leading the electrolyte denoted as FFL, characterized by an 3:3:2 FEC:FEMC:DME volume ratio and an overall Li salt concentration of 0.75 M and 0.5 wt% LiNO_3 . The electrolyte composition was extended to 1.0 M LiFSI in FEC:FEMC:DME (3:3:2 v/v) and 0.5 wt% LiNO_3 , which is referred to as FFD. For comparison, the conventional electrolyte 1.0 M LiPF_6 in EC:DEC (1:1 v/v) (referred to as LP30 and purchased from Duoduo Chemicals platform) was used.

The preparation of the $\text{LiNi}_{0.8}\text{Co}_{0.1}\text{Mn}_{0.1}\text{O}_2$ (NCM811) electrode involved mixing of the NCM811 powder, conductive carbon black, and poly(vinylidene-difluoride) (PVDF) in the weight ratio 92:4:4. 1-Methyl-2-pyrrolidinone (NMP) was used as solvent/dispersant to form the slurry, which was coated onto an Al foil. After vacuum drying at 120°C for 12 h, positive electrode discs (diameter of 12 mm) were punched. The average NCM811 positive electrodes was around 2.0 mg cm^{-2} . The same procedure was applied to prepare $\text{LiNi}_{0.91}\text{Co}_{0.06}\text{Mn}_{0.03}\text{O}_2$ (NCM90) electrodes with an areal loading around 22 mg cm^{-2} , which were used to assemble pouch cells. The activation process for the pouch cell included three steps, first 0.02 C charging for 2 h, then 0.05 C charging for 6 h, and finally charging at a constant current of 0.1 C up to 4.3 V.

2.2. Electrochemical measurements

The electrochemical tests were performed in CR2025 type coin-cells. Symmetric, $\text{Li}|\text{Li}$, and asymmetric, $\text{Li}|\text{Cu}$, and $\text{Li}|\text{NCM811}$, cells were assembled using the above-mentioned electrolytes. Cell assembly was carried out in an argon-filled glove box with a water and oxygen content of ≤ 0.01 ppm. The positive and negative electrodes were separated by a Celgard 2325 separator and 60 μL electrolyte were added. The Li deposition/stripping in all $\text{Li}|\text{Li}$ symmetric cell and $\text{Li}|\text{Cu}$ cell was fixed to 1 mAh cm^{-2} . $\text{Li}|\text{Li}$ symmetric cell were cycled at 1 mA cm^{-2} , 2 mA cm^{-2} , and 3 mA cm^{-2} , while the $\text{Li}|\text{Cu}$ cell were cycled only at 1 mA cm^{-2} . The $\text{Li}|\text{NCM811}$ electrodes were cycled at 0.1 C for the first formation cycle, then 10 cycles at 0.5 C to stabilize the interface with the electrolyte. All cells were tested at 25°C using a battery test system (Land, CT3002A, Wuhan, China). Electrochemical impedance spectroscopy (EIS) measurements were performed using an electrochemical workstation (CHI660E, Shanghai, China) over a frequency range of 10^5 – 10^{-2} Hz.

2.3. Materials characterization

The ion conductivity test was carried out using a DDSJ-308 F conductivity meter. Electrodes harvested from the tested cells inside an argon glove box were rinsed with DMC prior to further analysis. Raman spectra were obtained at room temperature using a Raman spectrometer (Renishaw inVia) equipped with a 785 nm laser. Deuterated chloroform (CDCl_3) was used as the solvent for recording ^1H NMR and ^{19}F NMR using nuclear magnetic resonance (NMR, AVANCE III HD 400 MHz). The morphology of deposited lithium metal and NCM811 particles was characterized using field-emission scanning electron microscopy (FESEM, Sigma 300VP). Copper current collectors (from $\text{Li}|\text{Cu}$ cells)

and positive electrodes (from Li||NCM811 cells) were investigated after prolonged cycling. The morphology of the solid electrolyte interphase (SEI) formed on NCM811 was analyzed using transmission electron microscopy (TEM, JEOL JEM-2100Plus, Japan). X-ray photoelectron spectroscopy (XPS) with Al K α X-ray radiation (ESCALAB 250Xi, Thermo Fischer, USA) was utilized to provide detailed information on the surface state and chemical composition of the materials.

3. Results and discussion

The structure of Li ions within the solvent and the desolvation behavior at the electrode/electrolyte interface play a crucial role in determining the performance of the electrode. Despite this, the composition and characteristics of the SEI film formed from the solvated structure have a significant impact on the overall cell performance. Thus, a thorough analysis of the solvation structure and composition is very important. Inorganic-rich SEIs are generally considered to have better ionic conductivity and mechanical strength, contributing to improve the electrode interfacial stability [29]. According to this study, reducing the presence of solvent molecules and increasing the coordination of anions with Li⁺ are crucial aspects for increasing the inorganic ratio in the composition of the SEI. Raman spectroscopy was carried out to analyze the solvation structure of the electrolyte. Various solvents and electrolytes were investigated with a focus on analyzing the peak values within the 690–950 cm⁻¹ range. As shown in Fig. 1a and Fig. S3, the DME solvent exhibits two C–O–C bending peaks associated with free

solvent molecules at 820 and 846 cm⁻¹ [30]. Regarding the FEC solvent, three peaks appeared at 729, 865 and 904 cm⁻¹, corresponding to C–O, C–F, and C–C vibration, respectively [31], and two peaks were observed for the FEMC solvent at 836 and 904 cm⁻¹. When adding LiFSI salt, there is a remarkable peak shift, which indicates for the Li⁺ coordination with solvent. However, the peak shift is much smaller for FFD and FFL when including the little amount of LiNO₃. This indicates for LiNO₃ to suppress the coordination of solvent molecules with Li⁺ (Fig. S3). In LiFSI-DME electrolyte, the appearance of the S–N–S bending peak at 718 cm⁻¹ indicates for the presence of free FSI⁻ [32,33]. After combining LiFSI and LiNO₃ with the various solvents to form the electrolytes, the content of free FSI⁻ anions decreased (Fig. 1b and Fig. S4) while the emergence of peaks around 726 cm⁻¹ and 738 cm⁻¹ suggests that more CIPs and AGG-I (one FSI⁻ coordinated with two Li⁺) and AGG-II (one FSI⁻ coordinated with multiple Li⁺) are formed in the electrolyte. It is worth noting that, compared to FFD, lower concentrations of FFL also exhibit lower coordination between Li⁺ and anions, which may be due to the excess solvent molecules winning the competition to coordinate with Li⁺. This indicates that an appropriate increase in concentration facilitates the Li⁺-FSI⁻ coordination [34–37], meanwhile, the involvement of a little amount of LiNO₃ can adjust the solvation structure, possibly promoting the formation of SEI rich in LiF and Li₃N components.

Nuclear magnetic resonance (NMR) was employed to investigate the interactions between solvents, anions, and lithium ions. As shown in Fig. 1c and Fig. S5, the interactions between solvents and electrolytes were explored based on the different chemical shifts. A single peak is

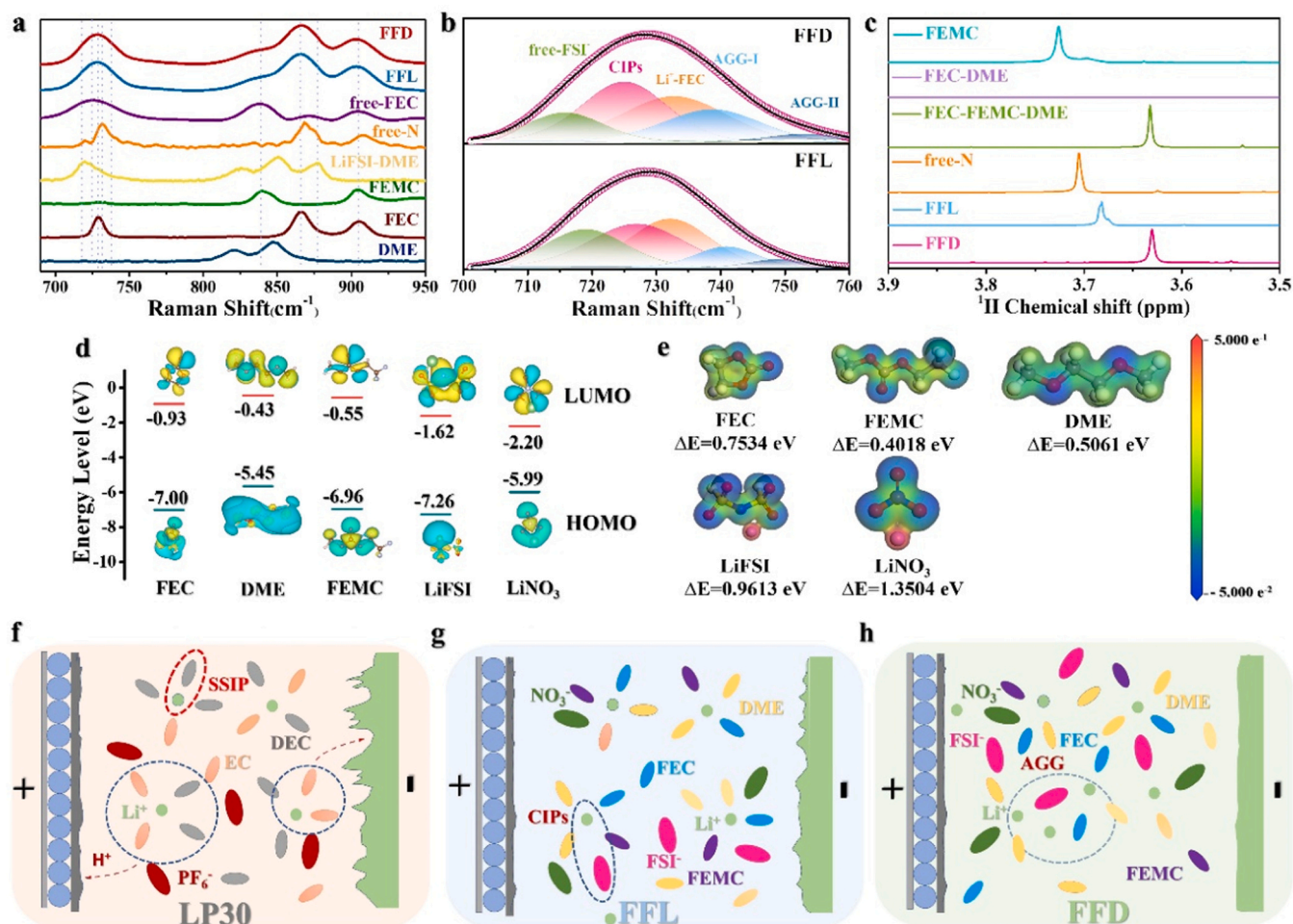


Fig. 1. a) Raman spectra in the range of 680–950 cm⁻¹, b) Raman spectra of electrolytes and their solvent molecules distribution, c) ¹H NMR results of various solvents and electrolytes, d) HOMO and LUMO energy levels of each component in the electrolyte, e) Adsorption energy between solvents and two lithium salts with Li⁺. Schematic representation of solvation structure between anode and cathode: f) LP30, g) FFL, h) FFD.

observed at 3.73 ppm, which is attributed to the $-\text{CH}_2$ group of FEMC. Two peaks are observed in FEC solvent at 6.15 ppm and 6.30 ppm, which are attributed to the $-\text{CH}-\text{CH}_2$ group of FEC. In the FEC-DME co-solvent, two peaks appeared at 3.10 ppm and 3.26 ppm, which are unique to DME and attributed to the $-\text{CH}_2-\text{CH}_2$ group. In Fig. S5, the FEC-DME co-solvent obviously shifted to high-field due to the strong solvating ability of DME, which increased the shielding effect and electron density. Upon the addition of FEMC solvent, i.e., having three different co-solvents, it is found that the peaks of FEC and DME both shifted to low field. This is attributed to the strong electronegativity of the $-\text{CF}_3$ group in FEMC, which attracts nearby electrons and decreases the electron density. Upon LiFSI added (sample named free-N), these peaks shift further towards lower fields, demonstrating that the solvents molecules coordinate with Li^+ . This resulted in a more pronounced weakening of hydrogen bonds causing a significant shift towards higher fields [35,38] due to the decrease of intermolecular distances. Interestingly, after introducing LiNO_3 (FFL and FFD), the peaks experienced a shift towards higher fields due to a competition between solvent molecules and NO_3^- ions. In particular, NO_3^- anions replace some of the solvent molecules involved in the coordination of lithium ions, causing a regression of the $\text{CH}-\text{CH}_2$ peak intensities for FEC and DME. The result suggests a weakening of the coordination between solvent molecules and lithium ions, allowing for a greater participation of anions (i.e., FSI^- , NO_3^-) to the lithium-ion coordination. However, at low concentrations of FFL, the reduced concentration of FSI^- ions results in an insufficient amount to compete with solvent molecules for coordination. Similar changes were observed in ^{19}F NMR, as shown in Fig. S5c, shows three peaks caused by the $-\text{CF}_3$ group in FEMC. Upon the addition of LiFSI, Li^+ coordinates with solvent molecules and anions, causing a shift in the electron cloud density around the F atoms [36,39]. Similarly, upon the addition of LiNO_3 , NO_3^- interacts with solvent molecules, further altering the distribution of the electron cloud around F atoms. Thus, following the NMR analysis, it is evident that the introduction of LiNO_3 increases the coordination of lithium ions by anions.

Density functional theory (DFT) was employed to calculate the energy levels of HOMO and LUMO, to gain insights into the redox properties of the electrolytes. Fig. 1d illustrates a comparison of the energy levels of the solvents and lithium salts. It can be observed that FEC, FEMC and LiFSI exhibit lower HOMO energy levels, indicating enhanced oxidation stability, i.e., reduced decomposition by oxidation. Conversely, LiNO_3 has higher HOMO energy levels, implying a lower oxidation stability and a propensity for oxidation, which contributes to the formation of an inorganic passivation layer on the positive electrode surface. This inorganic-rich layer is expected to enhance the toughness of the CEI and exhibit high ionic conductivity, facilitating ion transport within the CEI. Meanwhile, the same applies to LUMO energy levels where LiNO_3 owns the lowest. Further evidence supports the conception that LiNO_3 can undergo preferential oxidation and reduction, leading to the formation of inorganic-rich and poorly electron conductive passivation layer on the surface of both electrodes, possibly inhibiting electrolyte decomposition and improving the cycling life of the battery. Fig. 1e shows the potential energy of Li^+ adsorption, providing insights into the strength of the interaction between solvents and anions with lithium ions. The adsorption energy of both lithium salts is higher than that of a single solvent, indicating a stronger coordination with lithium ions. However, adsorption energy also has a certain impact on solubility, as strong binding to lithium ions restricts the participation of other molecules in coordination. Notably, LiNO_3 exhibits the highest adsorption energy, which correlates with its relatively low solubility in the electrolyte.

The solvation structure is evaluated based on the results depicted in Fig. 1f-h. In LP30 electrolyte, the strong solvating abilities of EC and DEC lead to the dominance of solvent molecules in the first solvation sheath [40]. This results in the formation of a large number of SSIP, which decomposition at the electrode surface leads to the development of a rich organic SEI layer with weak ionic conductivity and low

mechanical strength. Additionally, the strong interaction between Li^+ and solvent molecules increases the dissociation energy barrier for lithium ions. This implies that during the charging process of the battery, lithium ions need to overcome higher energy barriers to dissociate from solvent molecules, thereby promoting the growth of lithium dendrites [39]. For the FFL electrolyte (Fig. 1g), i.e., low salt concentration, solvent molecules primarily coordinate with Li^+ , but the presence of NO_3^- influences the solvation sheath, leading to the formation of more CIPs. This competition with solvent molecules promotes the coordination of FSI^- with Li^+ , inhibiting the reaction between FSI^- and the positive electrode interface, and reducing the formation of byproducts. However, the high HOMO level of DME makes it more susceptible to oxidation, resulting in a high organic content on the passivation layer over the positive electrode surface. Fortunately, NO_3^- has a similar HOMO level to DME. Thus, the prior decomposition of NO_3^- anion can form a passivation layer on both the cathode and anode surfaces, slowing down the decomposition of DME and, also, FEC and FEMC. Nonetheless, at low salt concentrations, the growth of lithium dendrites cannot be completely suppressed. However, there is still a significant improvement compared to the LP30 electrolyte. The FFD electrolyte with increased salt concentration addresses the issues (Fig. 1h). It achieves sufficient coordination between FSI^- and Li^+ , significantly reducing the decomposition of the electrolyte's solvent. Consequently, it improves the stability of the positive electrode structure, facilitating the formation of inorganic SEI components, e.g., LiF and Li_3N , and greatly improving battery stability.

The cycling stability of the $\text{Li} \parallel \text{Li}$ symmetric cells employing the three electrolytes was compared (see Fig. S6). The cell with FFD exhibited superior reversibility and lower polarizations compared to those employing LP30 and FFL. The result revealed the instability of the cell employing the conventional electrolyte (LP30) from the beginning of the cycling test accompanied by a significant polarization, ending in short circuit after 400 h of cycling. In contrast, the cell with free-N (without adding LiNO_3 salt) showed the lowest initial polarization, but growing faster than that of the one employing FFD. This observation highlights the stabilizing effect of LiNO_3 and the ability of FFD symmetric cells to cycle steadily for over 1000 h at 1 mA cm^{-2} . At 2 mA cm^{-2} , the initial potential of FFD was around 80 mV, approaching 200 mV after 500 cycles (Fig. 2a). This indicates that an almost ideal SEI layer formed on the lithium metal surface, which improved the cycling life and reduced the interfacial impedance. Conversely, the severe side reaction between lithium metal and conventional electrolytes results in unsatisfied passivation layer and increased polarization. Moreover, excessive electrolyte loss and the formation of dead lithium increased the resistance of the cell, which experienced a sudden rise in polarization after 100 cycles. With a further increase in current density to 3 mA cm^{-2} , it was found that only FFD maintained stable cycling with a polarization voltage of 100 mV, while LP30 experienced a gradual increase in polarization, leading to short circuit occurring after only 40 h (Fig. 2b). The rate performance of the symmetrical cells employing the three electrolytes was also evaluated (Fig. 2c). With LP30, the cell exhibited a rapid increase in polarization with increasing rates, and a short circuit occurring at 6 mA cm^{-2} . On the contrary, the two fluorinated electrolyte-based cells cycled stably even at 6 mA cm^{-2} and 8 mA cm^{-2} . However, it can be obviously seen that FFD demonstrates more notable performance, with the cell's polarization potential consistently lower than that of the FFL-based cell throughout the entire cycling process.

To evaluate the reversibility of the Li plating/stripping process, $\text{Li} \parallel \text{Cu}$ cells were conducted as shown in Fig. 2d and Fig. S7 and Fig. S8. The initial coulombic efficiency (ICE) of the FFD-based cell reached a high value of 95.2 %, surpassing the value of the FFL- (94.6 %), free-N- (92.7 %) and LP30- (94.5 %) based cells. In the subsequent cycles, the FFD-based cell showed a stable behavior resulting from the formation of a stable SEI and leading to continuously increasing Coulombic efficiency. The average Coulombic efficiency (CE) reached 96.0 % in 150 cycles, which is rather promising, but still low for "anode-less" lithium metal

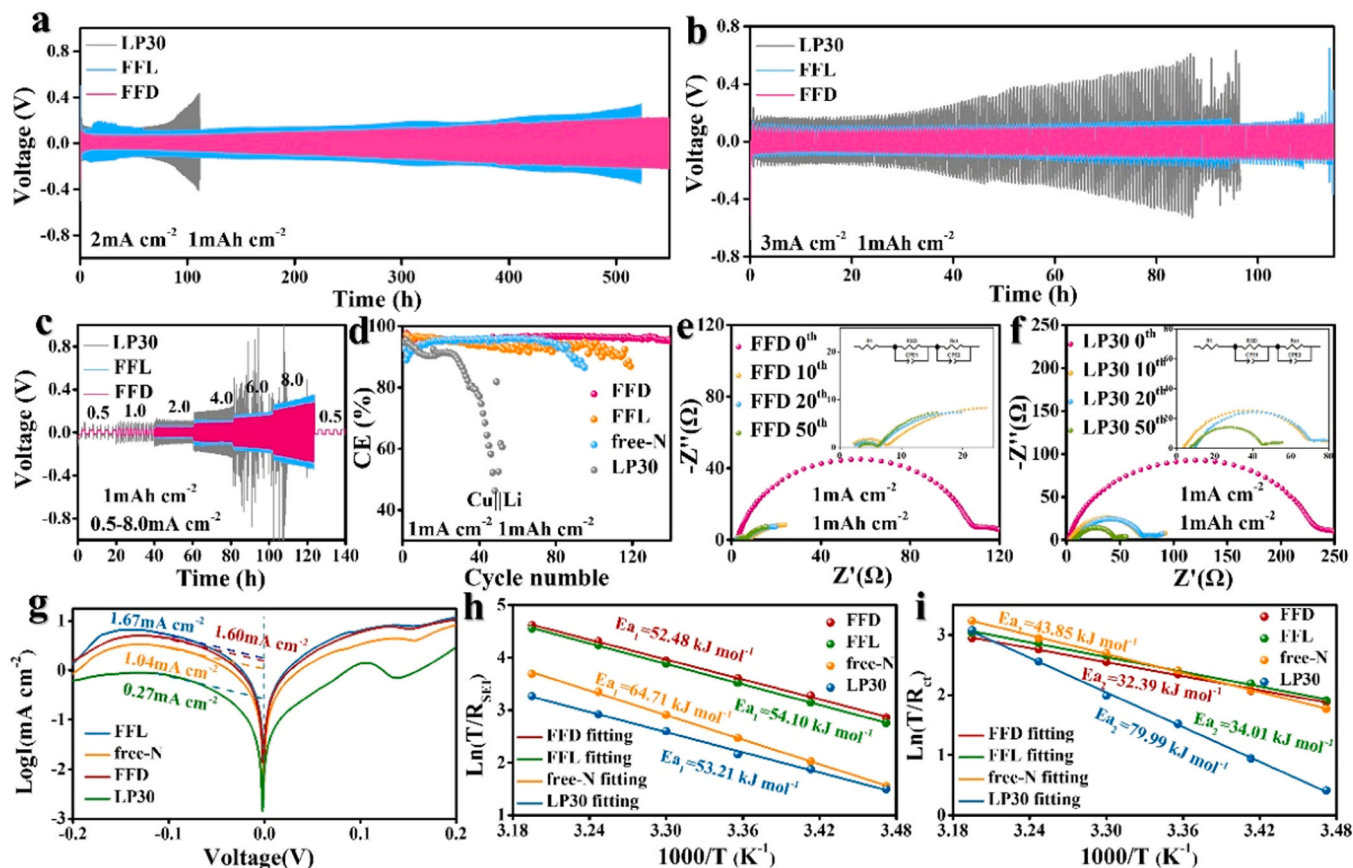


Fig. 2. a) Time-voltage curves of Li||Li symmetric cell in different electrolytes at 2 mA cm^{-2} , 1 mAh cm^{-2} and b) at 3 mA cm^{-2} , 1 mAh cm^{-2} . c) Rate performance of the electrolytes at current densities ranging from 0.5 to 8.0 mA cm^{-2} . d) Coulombic efficiency of a Li||Cu cell operating at 1 mA cm^{-2} and 1 mAh cm^{-2} . EIS spectrum of Li||Li symmetric cell measured in FFD e) and LP30 f) electrolytes at 1 mA cm^{-2} , 1 mAh cm^{-2} . g) Tafel curves of symmetric Li||Li cell in different electrolytes. h) and i) Activation energies of R_{SEI} and R_{ct} derived from Nyquist plots of cycled Li||Li symmetric cells with different electrolytes.

cells. However, FFD shows a significant improvement compared to free-N, which failed only after 80 cycles. This also indicates that the addition of trace amounts of LiNO_3 can greatly enhance cycling stability, potentially fostering the formation of a SEI rich in Li_3N components. In contrast, the growth of lithium dendrites in LP30 led to the generation of dead lithium, resulting in the continuous decrease of CE, rendering the cell incapable of supporting long-term cycling. The deposition/stripping curves of the electrolytes in Fig. S8 further demonstrate that FFD exhibits a smaller polarization potential and high reversibility upon Li plating/stripping. Fig. 2e, f, and Fig. S9 show the electrochemical impedance spectroscopy (EIS) after different cycles to investigate the interface stability of the lithium metal anode and electrolyte. FFD exhibited a significant decrease in impedance compared to LP30. This difference is due to the formation of a stable interfacial layer, as well as the generation of high ion conductive compounds, i.e., LiF and Li_3N , which greatly improved lithium-ion transport through the interface. Fig. 2g shows the Tafel curves of the electrolytes. The results revealed that FFD and FFL yielded higher exchange current density (J^0), 1.60 mA cm^{-2} and 1.67 mA cm^{-2} , respectively, whereas free-N exhibited a J^0 value of 1.04 mA cm^{-2} , and LP30 only stood at 0.27 mA cm^{-2} . The significant increase in J^0 indicates that FFD/FFL offer faster Li^+ transfer kinetics [41,42]. We know that in the Li plating/stripping process, Li^+ needs to overcome the energy barrier through the SEI layer and Li^+ solvation/desolvation. To evaluate the activation energies (represented as E_{a1} and E_{a2}) of R_{SEI} and R_{ct} , the electrochemical impedance spectra (EIS) of symmetric Li||Li cells were measured at different temperatures after 10 cycles. (Table S1, Fig. S10) [43]. The activation energy curves are shown in Fig. 2h and i, as shown in Fig. 2h, FFD has a lower E_{a1} value, indicating that the coordination of Li^+ by the

anions in the solvation shell significantly affects the SEI structure and composition, enhancing the Li^+ transfer kinetics. In Fig. 2i, the energy barrier for Li^+ desolvation is found to be large in free-N, but significantly reduced after the addition of LiNO_3 , as evidenced by the significant decrease in E_{a2} . This suggests that the addition of LiNO_3 regulates the environment of the Li^+ solvation shell and significantly enhances the Li^+ desolvation kinetics. In summary, FFD exhibits excellent compatibility with the lithium metal anode and demonstrates outstanding performance characteristics, including improved cycling stability, ion transport kinetics, and Coulombic efficiency.

The morphology of lithium deposited on copper foil at 1 mA cm^{-2} (1 mAh cm^{-2}) was characterized by SEM. FFD led to denser and more uniform lithium deposits (Fig. 3a–c) compared to LP30, which led to the formation of needle-like lithium instead (Fig. 3d–f). The bulk Li particles obtained in FFD own a reduced surface area, minimizing byproducts generation, thus contributing to better reversibility of the process. Despite the formation of blocky lithium deposits in FFL (see Fig. S11), large pores, i.e., low density, and some needle-shaped Li are observed (Fig. S11b and S11c). After ten cycles, a dense structure formed on the Li surface deposited in FFD (Fig. S12a), while many filamentous structures formed in LP30 (Fig. S12b). These observations further highlight the improved Li deposition performance, including reversibility and stability, achieved with FFD electrolyte compared to LP30.

The XPS curves in Fig. 3g–i provide insights into the elemental composition of the Li metal surface. Regarding the peaks in the C1s spectra (Fig. S13a), both electrolytes exhibit a strong peak at 284.8 eV , which is attributed to C–C/C–H bonds [44]. However, the C–O peak at 286.7 eV is stronger for LP30, indicating for the more extensive decomposition of the electrolyte's solvents, EC and DEC [45]. The peaks

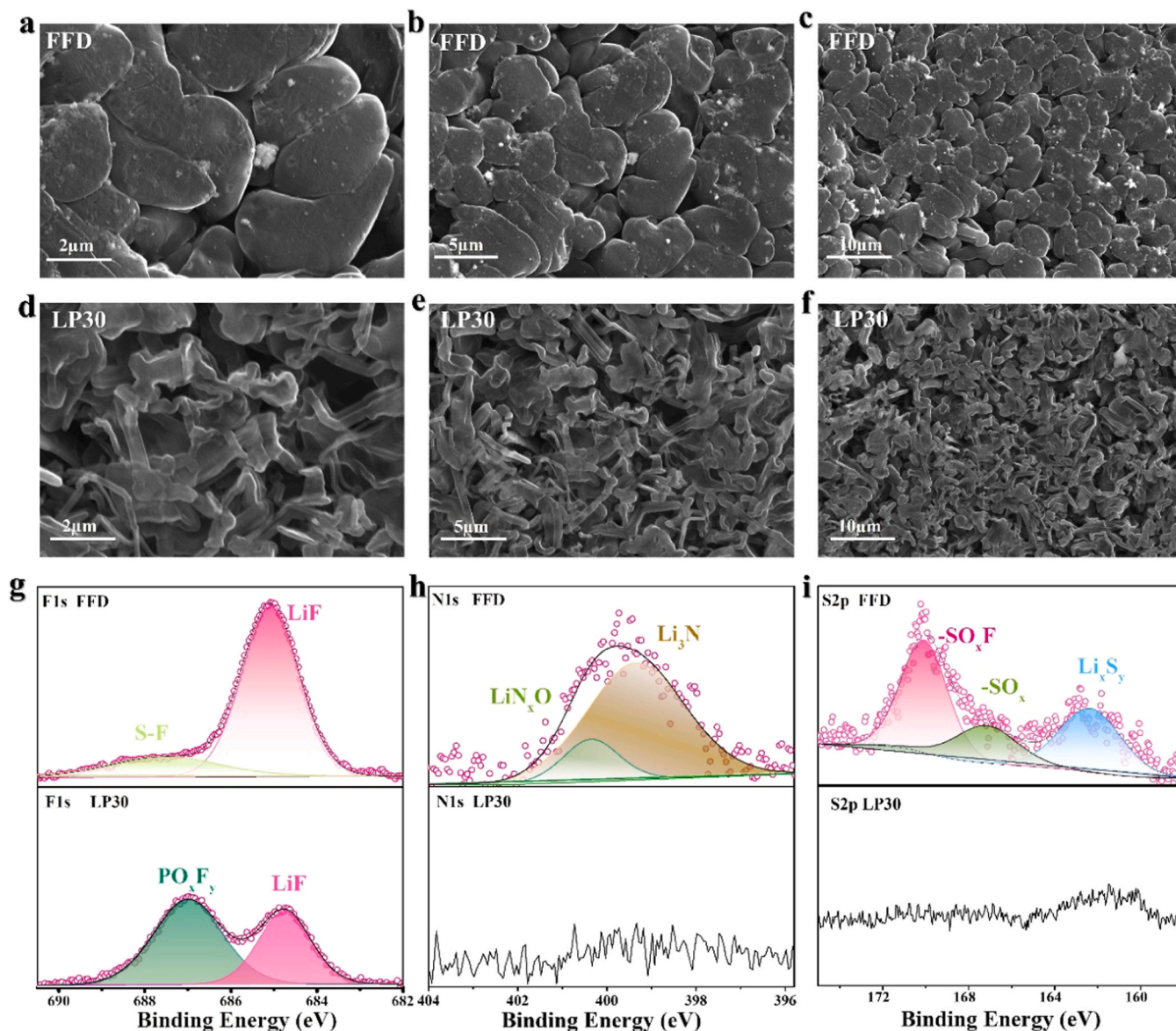


Fig. 3. Characterization of Li deposition morphology and surface composition. a-c) and d-f) show SEM images of the initial deposition morphology of Li in FFD and LP30. g-i) show XPS spectra of F1s, N1s, and S2p on the Li metal surface after 10 cycles in Li||Li symmetric cells with the two electrolytes.

at other positions show minimal differences between the two electrolytes. The Li_2CO_3 peak intensity during the initial cycle in FFD (Fig. S14a and S14b) is weak, indicating that the interaction between solvent molecules and the Li metal surface is suppressed during the initial deposition. The O1s spectra show peaks corresponding to C-O, Li_2CO_3 and C=O, which is consistent with the C1s spectra (Fig. S13b). Significant differences between the two electrolytes are observed in the F1s spectrum (Fig. 3g). A higher intensity of the LiF peak located at 685.1 eV is seen with FFD than the conventional electrolyte [46], supporting for an inorganic richer SEI in the former electrolyte, which provides better protection against further electrolyte/lithium metal reaction. In LP30, LiF was the main product during the initial deposition (Fig. S14c). However, as the cycling proceeded, the peak shifted towards PO_xF_y , indicating a significant decomposition of the electrolyte and formation of more by-products. This characteristic is also reflected in the Li1s spectra, as shown in Fig. S13c and S15. Although there are evident peaks indicating the presence of organic components in the C and O spectra in FFD electrolyte, the Li spectra show a high content of inorganic components, primarily LiF. Moreover, the presence of the Li_2O peak at 54.06 eV further indicates that the formed SEI has a high interfacial

energy, which is beneficial for its stability and passivation properties [47]. From the N1s and S2p spectra in Fig. 3h, i, and Fig. S16, it can be observed that decomposition occurs in both salts, LiFSI and LiNO_3 [44, 48]. The main decomposition products observed are Li_3N and Li_xS_y . These compounds own high ionic conductivity [49], which can improve lithium-ion transport contributing to the long-term cycling stability of cells. By performing XPS compositional analysis on the Li surface, it is clearly seen that FFD primarily generates inorganic components, i.e., LiF, Li_3N , Li_xS_y and Li_2O during cycling. These inorganic components collectively form a stable SEI, significantly improving the cycling stability and lifespan of the cell.

The performance of Li||NCM811 cell was tested with the various electrolytes. Fig. 4a shows the performance of the cells cycling within the voltage range of 3.0–4.3 V under 1 C rate (1 C=200 mAh g^{-1}) for 500 cycles. The one employing FFD demonstrated excellent cycle stability and long cycle life, achieving a high discharge capacity of 141.1 mAh g^{-1} after 500 cycles with 80 % capacity retention (based on the first discharge capacity of 176.4 mAh g^{-1} at 1 C). In contrast, FFL performed relatively poorly, showing a significant capacity decrease after 350 cycles. This could be attributed to the low Li salt concentration, resulting

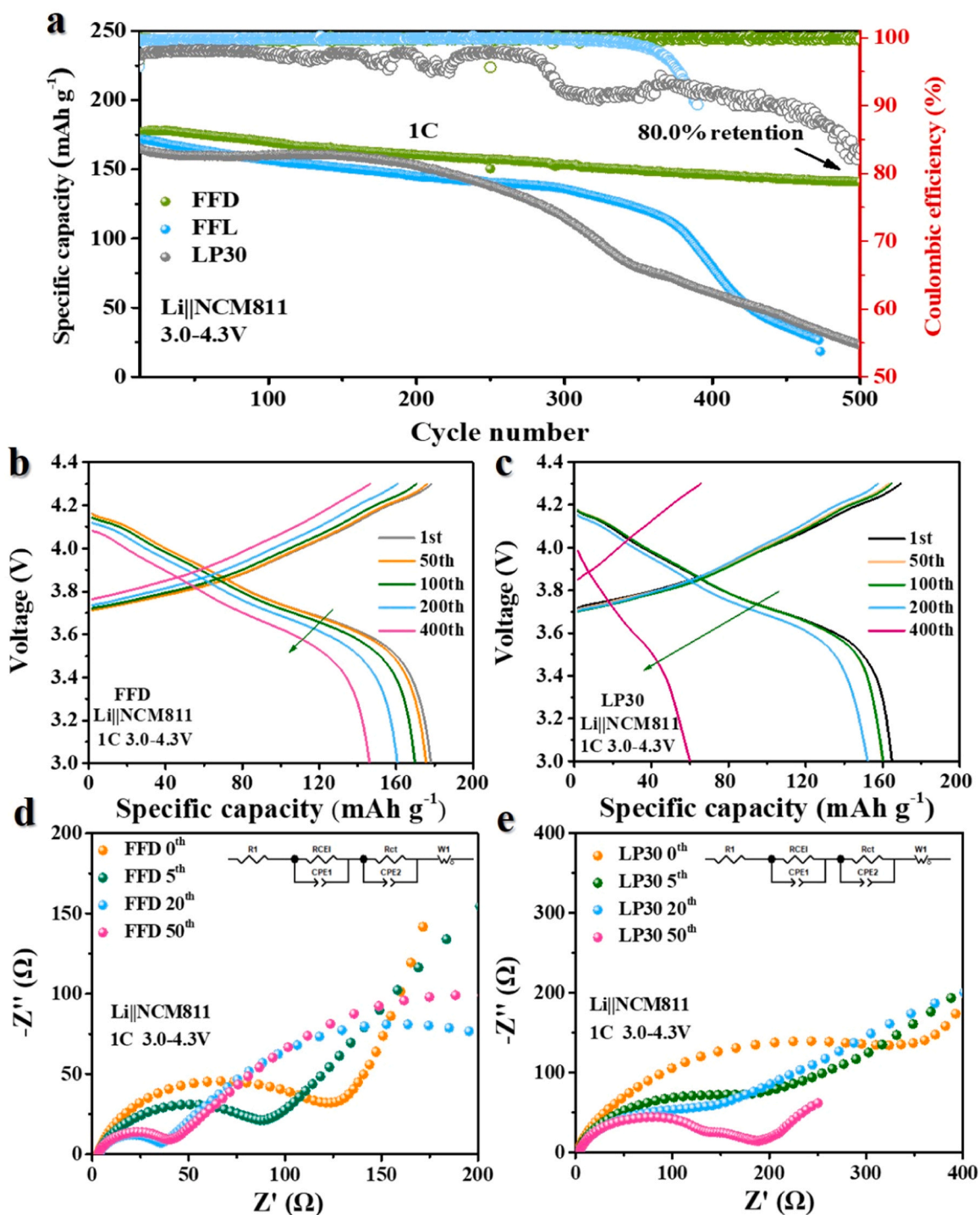


Fig. 4. Li||NCM811 cell electrochemical performance. a) First formation cycle at 0.1 C, ten cycles at 0.5 C, then 500 cycle at 1 C. b) and c) Selective charge-discharge curves during long cycling at 1 C at 4.3 V. d) and e) EIS measurement of the cell with different electrolyte after selected cycles.

in a large number of solvent molecules coordinating lithium ions, and the high HOMO level of DME, making it prone to oxidation, leading to the formation of more organic components in the CEI, ultimately causing reduced stability and capacity decay. Even worse, significant capacity decline occurs as early as 200 cycles using LP30 due to severe decomposition of electrolyte resulting in unstable electrode-electrolyte interface, increasing the cell resistance and hindering internal ion transfer. From the charge-discharge curves (see Fig. 4c) it is seen that the cell employing LP30 demonstrated a decent stability for the first 200 cycles, followed by a capacity fading upon further cycling. On the other

hand, the cell employing FFD remained stable throughout the cycling test (see Fig. 4b). Additionally, higher mass loading (7 mg cm^{-2}) NCM811 electrodes were tested. As illustrated in Fig. S17, it is evident that the cell employing FFD retains 83.6 % of its initial capacity after 200 cycles. In contrast, LP30 experiences severe electrolyte decomposition after 50 cycles. These results further confirm that FFD exhibits excellent compatibility with the positive electrode and possesses higher ionic conductivity. The impedance test of the cells after selected numbers of cycles is shown in Fig. 4d and e. The FFD cell showed always a lower impedance with respect to the LP30 cell, demonstrating a lower

resistance for lithium ions diffusion through the electrolyte/electrode interfaces due to the formation of more stable, i.e., thinner, CEI and SEI. The sum of the interfacial impedance actually decreased upon the initial 20 cycles and remained almost unchanged from the 20th to the 50th cycle, reflecting excellent stability. In contrast, the LP30 cell does not show a stable impedance, including a neat split of the features relative to the two interfaces after 50 cycles.

Increasing the cutoff voltage is a direct method to increase the discharge capacity and energy density. However, the inclusion of DME in the electrolyte diminishes its oxidation stability. When charging a Li||NCM811 cell with free-N electrolyte, the voltage reached an upper limit at 4.2 V before decreasing (Fig. S18a), indicating that its oxidation potential is insufficient to meet the standards for high-voltage applications. Fortunately, the addition of a small amount of LiNO₃ significantly increased the oxidation potential and improving the electrochemical stability, enabling it to operate in the high-voltage region (Fig. S18b).

Fig. 5a and S19 depicts the cycling performance of Li||NCM811 cells with the higher voltage cut-off set at 4.4 V and 4.5 V, respectively. With the former cut-off voltage, the FFD cell still exhibited great cycling stability, showing ICE of 91.2 % and 72.6 % capacity retention after 500 cycles while the LP30 cell only retained 41.1 % capacity after 500 cycles. With the 4.5 V cut-off voltage, the FFD cell demonstrated a discharge capacity of 217.1 mAh g⁻¹ (at 0.1 C) and a good capacity retention of 79.2 % after 300 cycles at 1 C (Fig. 5b and Fig. S20). To verify the electrochemical performance of FFD cells at high rates, rate tests were conducted from 0.1 C to 8 C. As shown in Fig. S21, FFD cells maintained high capacities even at high rates, particularly at 4 C. Thus, the FFD cells were subjected to long-term cycling at 2 C and 4 C (Fig. S22 and Fig. 5c-d). At 2 C rate, the FFD cell delivered 80.4 % of the capacity detected in the first cycle at such a rate, after 500 cycles. Remarkably, the cell exhibited excellent cycling performance even upon tests at 4 C rate, with an ICE of 90.4 %, and high average CE of 99.88 % and capacity

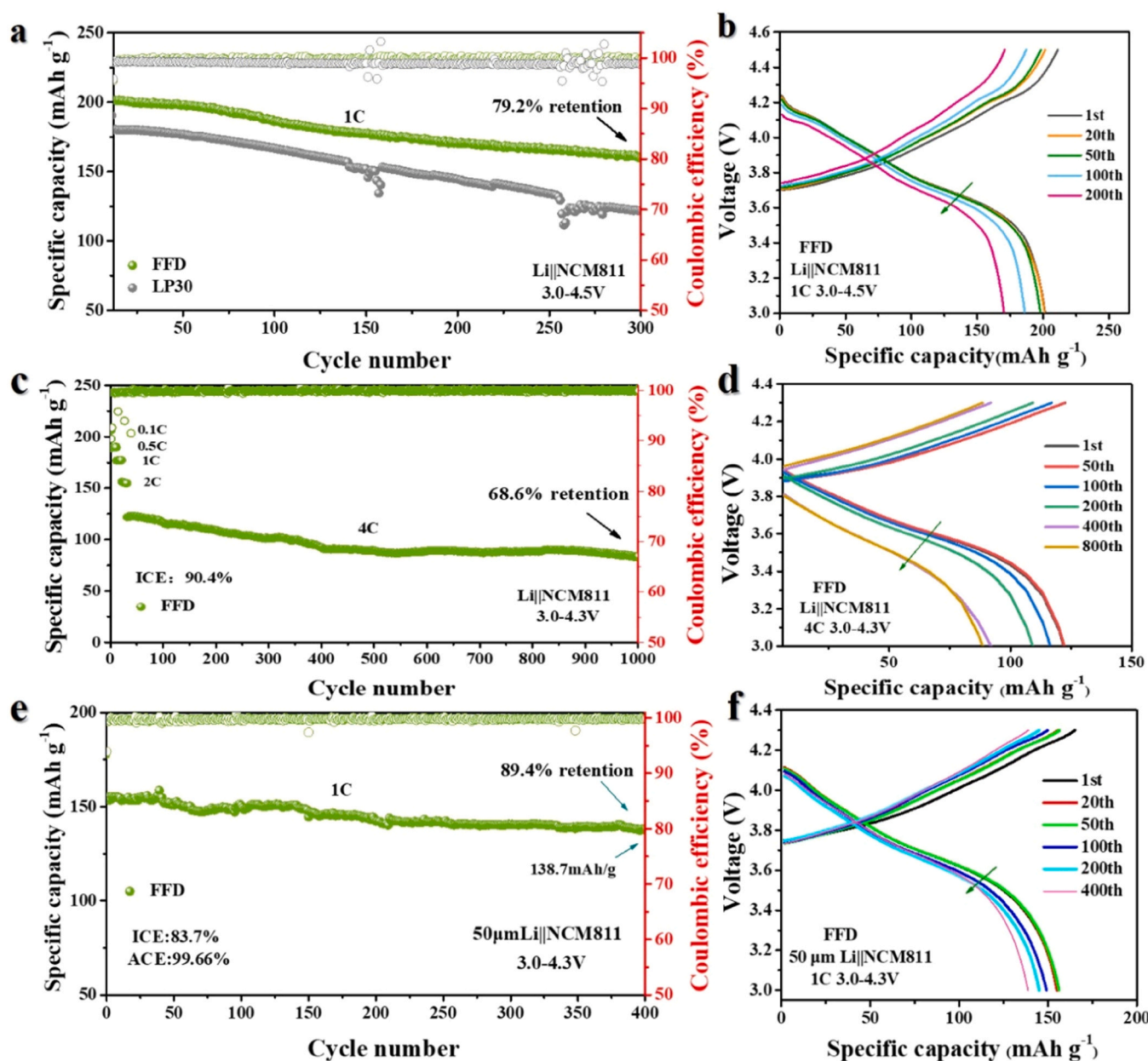


Fig. 5. a, b) The Li||NCM811 cell cycled at a high cutoff voltage of 4.5 V at 1 C rate and corresponding charge-discharge curves. c) Long-term cycles conducted at 4 C rate and d) selected charge-discharge curves during long-term cycling. e) Cycling performance of a Li||NCM811 full cell, employing a 50 µm-thick lithium electrode, assembled with FFD at 4.3 V and f) selected charge-discharge curves during long-term cycling at 1 C.

retention of up to 68.6 % after 1000 cycles. This highlights the excellent cycling stability of the FFD cell deriving from the electrolyte. Moreover, it exhibited incredible performance when used to assemble Li||NCM811 cell with a thin (50 μm) Li metal foil (Fig. 5e, f). The average coulombic efficiency of these cells reached the impressive value of 99.66 % while the capacity retention stayed at 89.4 % after 400 cycles at 1 C rate. These results highlight the superiority of FFD in terms of compatibility with both the positive and negative electrodes. Benefiting from the excellent performance of the full cell, a pouch cell was constructed to assess the potential use of FFD as an electrolyte for high-capacity lithium metal batteries. As depicted in Fig. S23, the pouch cell showcased a capacity of 1200 mAh, highlighting the promising application of FFD in high-energy-density lithium metal batteries.

To investigate the reason for the excellent electrochemical performance of the Li||NCM811 employing FFD as the electrolyte, the structural evolution and composition of the positive electrode material after 100 cycles at 1 C were further characterized. The TEM results demonstrate that a uniform CEI layer with a thickness of 4.21 nm formed on the recovered NCM811 particles, as shown in Fig. 6a and Fig. S24. The diffraction spectrum, obtained by Fourier Transform (FFT) analysis (Fig. S25), indicated that the layered structure and lattice spacing in the NCM811 particles was maintained when cycled with FFD [50]. On the contrary, the use of LP30 resulted in the formation of an uneven CEI layer with a thickness of 11.27 nm (Fig. 6b), accompanied by a significant degradation of the layered structure into the NiO rock-salt phase (Fig. S25b) [51,52]. This phenomenon can be primarily attributed to the

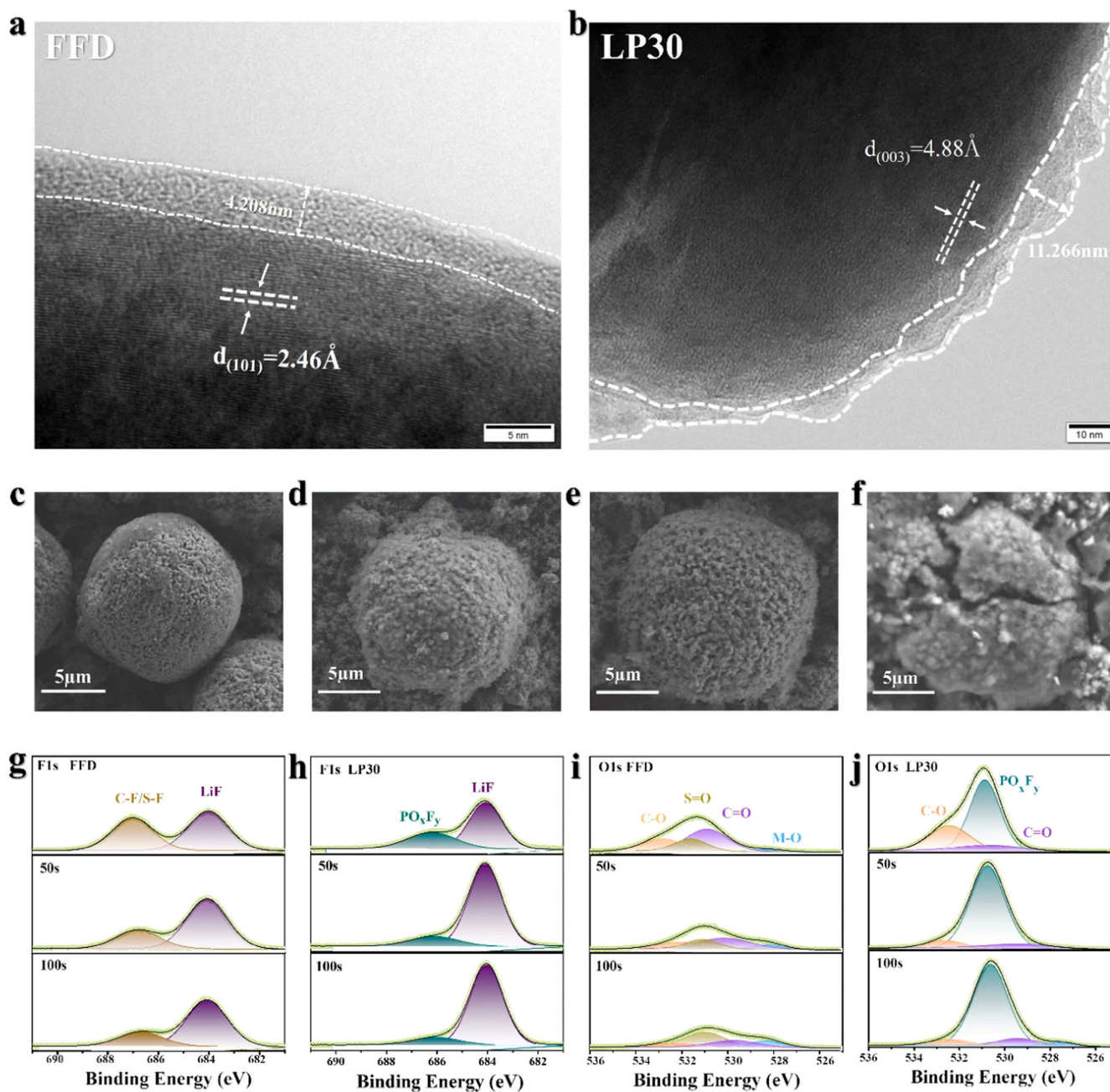


Fig. 6. Characterization of surface morphology and chemical composition of NCM811 cathode material. a) and b) are TEM images of NCM811 cathode after 100 cycles at 1 C rate with FFD and LP30 electrolytes, respectively. SEM images of NCM811 cathode before cycling c) and after 500 cycles with FFD d), FFD e) and LP30 f) electrolytes, respectively. XPS spectra of NCM811 cathode after 100 cycles with different electrolyte at 0–120 s depth etching, F 1 s spectra from FFD g) and LP30 h); O 1 s spectra from FFD i) and LP30 j).

scarce protection offered by the CEI toward transition metal dissolution, among other effects, leading to the degeneration of the NCM811 structure and poor electrochemical performance (Fig. 4a, e).

Fig. 6c–f reports SEM images of the cathode material extracted from Li||NCM811 cells after 500 cycles. With the FFD electrolyte, the NCM811 particles remain intact, showing a dense surface covered by a compact CEI layer. However, in FFL, although the particles remain spherical, their surface is rough indicating for the inhomogeneity of the CEI, which results in the instability of the material structure and the electrochemical performance. Even worse, the NCM811 particles cycled in LP30 suffer severe damage, exhibiting cracks and pulverization, and significant disruption of the internal structure, resulting in the sharp capacity decline of the LP30 cell after 200 cycles.

XPS measurements were carried out to analysis the surface chemical composition of NCM811 electrodes after 100 cycles as shown in Fig. 6g–h. In the F1s spectra of the electrode cycled in FFD, a C-F/S-F peak at 687.0 eV and a LiF peak at 684.0 eV were observed [53,54]. The C-F/S-F peak is associated with a decomposition product of the FSI anion. Deep etching experiments revealed that the LiF content remained basically unchanged, but the C-F/S-F content decreased significantly [55]. As shown in Fig. S26a, the organic components in the outer CEI surface (toward the electrolyte) were relatively high, but the representative organic components such as C-F and C=O decreased significantly upon etching [44]. This reveals the formation of a highly stable dual-layered CEI, with the outer surface primarily composed of C-F and S-F rich organic components, and the inner part consisting mainly of LiF and Li₃N rich inorganic components. The organic layer on the surface effectively acts as a buffering layer, mitigating the stress caused by the inner layer. The inner layer, composed of inorganic components, exhibits high mechanical strength and ion conductivity, greatly enhancing interfacial stability and ion transport. These, in turn, ensures long-term cycling stability and high charge/discharge efficiency (Fig. 4a). Regarding the LP30 electrolyte (Fig. 6h), the content of LiF is found to increase with etching, which seems to be a positive development. However, as observed in Fig. S26b, the organic component content on its surface is remarkably low. This “anomalous phenomenon” can be explained as follows: in the electrolyte, the high dissociation energies of EC and DEC lead to weak Li⁺-PF₆⁻ interactions. The excess free PF₆⁻ ions are easily accessible to solvent molecules, inducing partial solvent polarization and altering the internal charge distribution. As a result, the electrons of H atoms in the solvent are partially removed, leading to dehydrogenation reactions that can easily damage the positive electrode structure and generate HF through reaction with PF₆⁻ [39]. The solvent pairs near the cathode surface preferentially coordinate with newly extracted Li⁺ from the positive material, and the adsorbed solvent may also oxidatively decompose to form Li₂CO₃, reacting with HF to form LiF [40]. Thus, the high LiF content observed in the compositional analysis results in the formation of a rigid and fragile CEI film, explaining the phenomenon of significant cracking in the positive particles after cycling. In the O1s region of the electrode tested in FFD, the S=O peak is associated with the occurrence of the FSI decomposition. However, as the etching depth increases, the S=O decreases, further supporting for the formation of a stable and thin CEI (Fig. 6i). In LP30, a significant amount of PO_xF_y decomposition products is observed, which is not reduced, but even enhanced at increasing etching depths. This indicates that extensive degradation of the electrolyte is occurring along the cycling, leading to the continuous thickening of the unstable CEI.

4. Conclusions

Through extensive research efforts, it is demonstrated as the FFD electrolyte exhibits remarkable performance and stability with the lithium metal anode. Moreover, The Li||NCM811 battery assembled with this electrolyte underwent multiple rate performance tests within a voltage window of 3.0–4.3 V, demonstrating excellent cycling stability and high energy efficiency. After 500 cycles at 1 C rate, the cell

maintained high capacity, 80.0 % retention, and an average coulombic efficiency of 99.76 %. Similarly, after 1000 cycles at 4 C rate, the battery retained 68.6 % of its capacity and an average coulombic efficiency of 99.88 %. Notably, even under the high voltage charge condition (4.5 V), the battery exhibited resilience to voltage instability, maintaining high capacity retention (79.2 %) after 300 cycles at 1 C rate. These results underscore the excellent compatibility of the FFD electrolyte with both the cathode and lithium metal anode, enabling the formation of a robust inorganic-rich SEI with high ionic conductivity and mechanical strength, thus enhancing interfacial stability. This research offers a valuable insight for the development of novel electrolyte for high performance lithium metal batteries.

CRediT authorship contribution statement

Rao Yuxin: Writing – review & editing, Writing – original draft, Investigation, Formal analysis, Data curation, Conceptualization. **Li Xue:** Writing – review & editing, Investigation, Formal analysis, Data curation. **Zhao Shangquan:** Writing – review & editing, Investigation, Formal analysis, Data curation. **Liu Pengfei:** Writing – review & editing, Investigation, Formal analysis, Data curation. **Wu Fanglin:** Writing – review & editing, Formal analysis. **Liu Xiang:** Writing – review & editing, Investigation, Formal analysis, Data curation. **Zhou Naigen:** Writing – review & editing, Formal analysis. **Fang Shan:** Writing – review & editing, Writing – original draft, Conceptualization. **Passerini Stefano:** Writing – review & editing, Supervision, Resources, Project administration, Funding acquisition, Conceptualization.

Declaration of Competing Interest

The authors declare that they have no known competing financial interests or personal relationships that could have appeared to influence the work reported in this paper.

Data Availability

Data will be made available on request.

Acknowledgments

Project funded by the Talent Project of National Natural Science Foundation of China (52161039, 52002176, 12305327) and Naigen Zhou (52062035). Double Thousands Plan in Jiangxi Province (jxsq2020101056), Jiangxi Provincial Natural Science Foundation (20212BAB214054, 20224BAB204011, 20224BAB214011, 20232BAB211028), SP acknowledges the support of the Helmholtz Association.

Appendix A. Supporting information

Supplementary data associated with this article can be found in the online version at [doi:10.1016/j.nanoen.2024.109362](https://doi.org/10.1016/j.nanoen.2024.109362).

References

- [1] G. Jiang, J. Liu, J. He, H. Wang, S. Qi, J. Huang, D. Wu, J. Ma, Hydrofluoric acid-removable additive optimizing electrode electrolyte interphases with Li⁺ conductive moieties for 4.5V lithium metal batteries, *Adv. Funct. Mater.* 33 (2023).
- [2] R. Wang, W. Cui, F. Chu, F. Wu, Lithium metal anodes: present and future, *J. Energy Chem.* 48 (2020) 145–159.
- [3] X.B. Cheng, R. Zhang, C.Z. Zhao, Q. Zhang, Toward safe lithium metal anode in rechargeable batteries: a review, *Chem. Rev.* 117 (2017) 10403–10473.
- [4] D. Lin, Y. Liu, Y. Cui, Reviving the lithium metal anode for high-energy batteries, *Nat. Nanotechnol.* 12 (2017) 194–206.
- [5] G. Zheng, S.W. Lee, Z. Liang, H.W. Lee, K. Yan, H. Yao, H. Wang, W. Li, S. Chu, Y. Cui, Interconnected hollow carbon nanospheres for stable lithium metal anodes, *Nat. Nanotechnol.* 9 (2014) 618–623.
- [6] W. Cao, Q. Li, X. Yu, H. Li, Controlling Li deposition below the interface, *eScience* 2 (2022) 47–78.

- [7] W. Zhang, T. Yang, X. Liao, Y. Song, Y. Zhao, All-fluorinated electrolyte directly tuned Li^+ solvation sheath enabling high-quality passivated interfaces for robust Li metal battery under high voltage operation, *Energy Storage Mater.* 57 (2023) 249–259.
- [8] Q. Wang, Z. Yao, C. Zhao, T. Verhallen, D.P. Tabor, M. Liu, F. Ooms, F. Kang, A. Aspuru-Guzik, Y.S. Hu, M. Wagemaker, B. Li, Interface chemistry of an amide electrolyte for highly reversible lithium metal batteries, *Nat. Commun.* 11 (2020) 4188.
- [9] X. Chen, Q. Zhang, Atomic insights into the fundamental interactions in lithium battery electrolytes, *Acc. Chem. Res.* 53 (2020) 1992–2002.
- [10] M.S. Kim, Z. Zhang, J. Wang, S.T. Oyakhire, S.C. Kim, Z. Yu, Y. Chen, D.T. Boyle, Y. Ye, Z. Huang, W. Zhang, R. Xu, P. Sayavong, S.F. Bent, J. Qin, Z. Bao, Y. Cui, Revealing the multifunctions of $\text{Li}(3)\text{N}$ in the suspension electrolyte for lithium metal batteries, *ACS Nano* 17 (2023) 3168–3180.
- [11] M.S. Kim, Z. Zhang, P.E. Rudnicki, Z. Yu, J. Wang, H. Wang, S.T. Oyakhire, Y. Chen, S.C. Kim, W. Zhang, D.T. Boyle, X. Kong, R. Xu, Z. Huang, W. Huang, S. F. Bent, L.W. Wang, J. Qin, Z. Bao, Y. Cui, Suspension electrolyte with modified Li^+ solvation environment for lithium metal batteries, *Nat. Mater.* 21 (2022) 445–454.
- [12] S. Liu, X. Ji, N. Piao, J. Chen, N. Eidson, J. Xu, P. Wang, L. Chen, J. Zhang, T. Deng, S. Hou, T. Jin, H. Wan, J. Li, J. Tu, C. Wang, An inorganic-rich solid electrolyte interphase for advanced lithium-metal batteries in carbonate electrolytes, *Angew. Chem. Int. Ed. Engl.* 60 (2021) 3661–3671.
- [13] J. Chen, Q. Li, T.P. Pollard, X. Fan, O. Borodin, C. Wang, Electrolyte design for Li metal-free Li batteries, *Mater. Today* 39 (2020) 118–126.
- [14] X. Fan, X. Ji, F. Han, J. Yue, J. Chen, L. Chen, T. Deng, J. Jiang, C. Wang, Fluorinated solid electrolyte interphase enables highly reversible solid-state Li metal battery, *Sci. Adv.* 4 (2018).
- [15] S. Liu, X. Ji, J. Yue, S. Hou, P. Wang, C. Cui, J. Chen, B. Shao, J. Li, F. Han, J. Tu, C. Wang, High interfacial-energy interphase promoting safe lithium metal batteries, *J. Am. Chem. Soc.* 142 (2020) 2438–2447.
- [16] M. Mao, X. Ji, Q. Wang, Z. Lin, M. Li, T. Liu, C. Wang, Y.S. Hu, H. Li, X. Huang, L. Chen, L. Suo, Anion-enrichment interface enables high-voltage anode-free lithium metal batteries, *Nat. Commun.* 14 (2023) 1082.
- [17] Y. Wang, Z. Li, Y. Hou, Z. Hao, Q. Zhang, Y. Ni, Y. Lu, Z. Yan, K. Zhang, Q. Zhao, F. Li, J. Chen, Emerging electrolytes with fluorinated solvents for rechargeable lithium-based batteries, *Chem. Soc. Rev.* 52 (2023) 2713–2763.
- [18] Z. Zeng, V. Murugesan, K.S. Han, X. Jiang, Y. Cao, L. Xiao, X. Ai, H. Yang, J.-G. Zhang, M.L. Sushko, J. Liu, Non-flammable electrolytes with high salt-to-solvent ratios for Li-ion and Li-metal batteries, *Nat. Energy* 3 (2018) 674–681.
- [19] F. Wu, Z. Chen, S. Fang, W. Zuo, G.-T. Kim, S. Passerini, The role of ionic liquids in resolving the interfacial chemistry for (quasi-) solid-state batteries, *Energy Storage Mater.* 63 (2023).
- [20] Y. Zou, Z. Ma, G. Liu, Q. Li, D. Yin, X. Shi, Z. Cao, Z. Tian, H. Kim, Y. Guo, C. Sun, L. Cavallo, L. Wang, H.N. Alshareef, Y.K. Sun, J. Ming, Non-flammable electrolyte enables high-voltage and wide-temperature lithium-ion batteries with fast charging, *Angew. Chem. Int. Ed. Engl.* 62 (2023).
- [21] X. Cao, P. Gao, X. Ren, L. Zou, M.H. Engelhard, B.E. Matthews, J. Hu, C. Niu, D. Liu, B.W. Arey, C. Wang, J. Xiao, J. Liu, W. Xu, J.G. Zhang, Effects of fluorinated solvents on electrolyte solvation structures and electrode/electrolyte interphases for lithium metal batteries, *Proc. Natl. Acad. Sci. U. S. A.* 118 (2021).
- [22] J. Zou, K. Yuan, J. Zhao, B. Wang, S. Chen, J. Huang, H. Li, X. Niu, L. Wang, Delithiation-driven topotactic reaction endows superior cycling performances for high-energy-density FeS_x ($1 \leq x \leq 1.14$) cathodes, *Energy Storage Mater.* 43 (2021) 579–584.
- [23] H. Lee, H.-S. Lim, X. Ren, L. Yu, M.H. Engelhard, K.S. Han, J. Lee, H.-T. Kim, J. Xiao, J. Liu, W. Xu, J.-G. Zhang, Detrimental effects of chemical crossover from the lithium anode to cathode in rechargeable lithium metal batteries, *ACS Energy Lett.* 3 (2018) 2921–2930.
- [24] E.M. Erickson, W. Li, A. Dolocan, A. Manthiram, Insights into the cathode-electrolyte interphases of high-energy-density cathodes in lithium-ion batteries, *ACS Appl. Mater. Interfaces* 12 (2020) 16451–16461.
- [25] H. Yang, X. Chen, N. Yao, N. Piao, Z. Wang, K. He, H.-M. Cheng, F. Li, Dissolution-precipitation dynamics in ester electrolyte for high-stability lithium metal batteries, *ACS Energy Lett.* (2021) 1413–1421.
- [26] C. Yan, Y.X. Yao, X. Chen, X.B. Cheng, X.Q. Zhang, J.Q. Huang, Q. Zhang, Lithium nitrate solvation chemistry in carbonate electrolyte sustains high-voltage lithium metal batteries, *Angew. Chem. Int. Ed. Engl.* 57 (2018) 14055–14059.
- [27] J. Fu, X. Ji, J. Chen, L. Chen, X. Fan, D. Mu, C. Wang, Lithium nitrate regulated sulfone electrolytes for lithium metal batteries, *Angew. Chem. Int. Ed. Engl.* 59 (2020) 22194–22201.
- [28] Y. Jie, X. Liu, Z. Lei, S. Wang, Y. Chen, F. Huang, R. Cao, G. Zhang, S. Jiao, Enabling high-voltage lithium metal batteries by manipulating solvation structure in ester electrolyte, *Angew. Chem. Int. Ed. Engl.* 59 (2020) 3505–3510.
- [29] J. Liu, M. Wu, X. Li, D. Wu, H. Wang, J. Huang, J. Ma, Amide-functional, $\text{Li}_3\text{N}/\text{LiF}$ -rich heterostructured electrode electrolyte interphases for 4.6V $\text{Li}||\text{LiCoO}_2$ batteries, *Adv. Energy Mater.* 13 (2023).
- [30] N. Sun, R. Li, Y. Zhao, H. Zhang, J. Chen, J. Xu, Z. Li, X. Fan, X. Yao, Z. Peng, Anionic coordination manipulation of multilayer solvation structure electrolyte for high-rate and low-temperature lithium metal battery, *Adv. Energy Mater.* 12 (2022).
- [31] G. Yang, R.L. Sacchi, I.N. Ivanov, R.E. Ruther, K.A. Hays, Y. Zhang, P.-F. Cao, G. M. Veith, N.J. Dudney, T. Saito, D.T. Hallinan, J. Nanda, Probing electrolyte solvents at solid/liquid interface using gap-mode surface-enhanced Raman spectroscopy, *J. Electrochem. Soc.* 166 (2019) A178–A187.
- [32] J. Wu, Z. Gao, Y. Tian, Y. Zhao, Y. Lin, K. Wang, H. Guo, Y. Pan, X. Wang, F. Kang, N. Tavajohi, X. Fan, B. Li, Unique tridentate coordination tailored solvation sheath towards highly stable lithium metal batteries, *Adv. Mater.* (2023) e2303347.
- [33] T. Li, X.Q. Zhang, N. Yao, Y.X. Yao, L.P. Hou, X. Chen, M.Y. Zhou, J.Q. Huang, Q. Zhang, Stable anion-derived solid electrolyte interphase in lithium metal batteries, *Angew. Chem. Int. Ed. Engl.* 60 (2021) 22683–22687.
- [34] Y. Liu, Y. Huang, X. Xu, Y. Liu, J. Yang, J. Lai, J. Shi, S. Wang, W. Fan, Y.P. Cai, Y. Q. Lan, Q. Zheng, Fluorinated solvent-coupled anion-derived interphase to stabilize silicon microparticle anodes for high-energy-density batteries, *Adv. Funct. Mater.* (2023).
- [35] S. Lei, Z. Zeng, H. Yan, M. Qin, M. Liu, Y. Wu, H. Zhang, S. Cheng, J. Xie, Nonpolar cosolvent driving LUMO energy evolution of methyl acetate electrolyte to afford lithium-ion batteries operating at -60°C , *Adv. Funct. Mater.* (2023).
- [36] G. Zhang, J. Li, Q. Wang, H. Wang, J. Wang, K. Yu, J. Chang, C. Wang, X. Hong, Q. Ma, Y. Deng, A nonflammable electrolyte for high-voltage lithium metal batteries, *ACS Energy Lett.* (2023) 2868–2877.
- [37] Y. Lin, Z. Yang, X. Zhang, Y. Liu, G. Hu, S. Chen, Y. Zhang, Activating ultra-low temperature Li-metal batteries by tetrahydrofuran-based localized saturated electrolyte, *Energy Storage Mater.* 58 (2023) 184–194.
- [38] Z. Jiang, Z. Zeng, X. Liang, L. Yang, W. Hu, C. Zhang, Z. Han, J. Feng, J. Xie, Fluorobenzene, a low-density, economical, and bifunctional hydrocarbon cosolvent for practical lithium metal batteries, *Adv. Funct. Mater.* 31 (2020).
- [39] Y. Zou, G. Liu, Y. Wang, Q. Li, Z. Ma, D. Yin, Y. Liang, Z. Cao, L. Cavallo, H. Kim, L. Wang, H.N. Alshareef, Y.K. Sun, J. Ming, Intermolecular interactions mediated nonflammable electrolyte for high-voltage lithium metal batteries in wide temperature, *Adv. Energy Mater.* 13 (2023).
- [40] R. Deng, F. Chu, F. Kwofie, Z. Guan, J. Chen, F. Wu, A low-concentration electrolyte for high-voltage lithium-metal batteries: fluorinated solvation shell and low salt concentration effect, *Angew. Chem. Int. Ed. Engl.* 61 (2022).
- [41] Q. Peng, Z. Liu, S. Chen, P. Duan, S. Cheng, L. Jiang, J. Sun, Q. Wang, Developing multifunctional amide additive by rational molecular design for high-performance Li metal batteries, *Nano Energy* 113 (2023).
- [42] S. Fang, F. Wu, S. Zhao, M. Zarrabeitia, G.T. Kim, J.K. Kim, N. Zhou, S. Passerini, Adaptive multi-site gradient adsorption of siloxane-based protective layers enable high performance lithium-metal batteries, *Adv. Energy Mater.* (2023).
- [43] W. Fang, Z. Wen, L. Chen, Z. Qin, J. Li, Z. Zheng, Z. Weng, G. Wu, N. Zhang, X. Liu, X. Yuan, G. Chen, Constructing inorganic-rich solid electrolyte interphase via abundant anionic solvation sheath in commercial carbonate electrolytes, *Nano Energy* 104 (2022).
- [44] Y. Lu, W. Zhang, S. Liu, Q. Cao, S. Yan, H. Liu, W. Hou, P. Zhou, X. Song, Y. Ou, Y. Li, K. Liu, Tuning the Li^+ solvation structure by a "Bulky Coordinating" strategy enables nonflammable electrolyte for ultrahigh voltage lithium metal batteries, *ACS Nano* 17 (2023) 9586–9599.
- [45] J. Zhang, H. Zhang, S. Weng, R. Li, D. Lu, T. Deng, S. Zhang, L. Lv, J. Qi, X. Xiao, L. Fan, S. Geng, F. Wang, L. Chen, M. Noked, X. Wang, X. Fan, Multifunctional solvent molecule design enables high-voltage Li-ion batteries, *Nat. Commun.* 14 (2023) 2211.
- [46] Z. Zhu, J. Ji, X. Qi, Y. Ji, Z. Liu, W. Du, Y. Pan, D. Yang, J. Ma, L. Qie, Y. Huang, Rational anion selection of the electrolyte additive for highly reversible lithium plating/stripping, *Adv. Energy Mater.* 13 (2023).
- [47] X. Wang, S. Wang, H. Wang, W. Tu, Y. Zhao, S. Li, Q. Liu, J. Wu, Y. Fu, C. Han, F. Kang, B. Li, Hybrid electrolyte with dual-anion-aggregated solvation sheath for stabilizing high-voltage lithium-metal batteries, *Adv. Mater.* 33 (2021).
- [48] C. Liao, L. Han, W. Wang, W. Li, X. Mu, Y. Kan, J. Zhu, Z. Gui, X. He, L. Song, Y. Hu, Non-flammable electrolyte with lithium nitrate as the only lithium salt for boosting ultra-stable cycling and fire-safety lithium metal batteries, *Adv. Funct. Mater.* 33 (2023).
- [49] P. Li, H. Zhang, J. Lu, G. Li, Low concentration sulfolane-based electrolyte for high voltage lithium metal batteries, *Angew. Chem. Int. Ed. Engl.* 62 (2023).
- [50] X. Ren, S. Chen, H. Lee, D. Mei, M.H. Engelhard, S.D. Burton, W. Zhao, J. Zheng, Q. Li, M.S. Ding, M. Schroeder, J. Alvarado, K. Xu, Y.S. Meng, J. Liu, J.-G. Zhang, W. Xu, Localized high-concentration sulfone electrolytes for high-efficiency lithium-metal batteries, *Chem* 4 (2018) 1877–1892.
- [51] W. Gu, G. Xue, Q. Dong, R. Yi, Y. Mao, L. Zheng, H. Zhang, X. Fan, Y. Shen, L. Chen, Trimethoxyboroxine as an electrolyte additive to enhance the 4.5V cycling performance of a Ni-rich layered oxide cathode, *eScience* 2 (2022) 486–493.
- [52] W. Xue, M. Huang, Y. Li, Y.G. Zhu, R. Gao, X. Xiao, W. Zhang, S. Li, G. Xu, Y. Yu, P. Li, J. Lopez, D. Yu, Y. Dong, W. Fan, Z. Shi, R. Xiong, C.-J. Sun, I. Hwang, W.-K. Lee, Y. Shao-Horn, J.A. Johnson, J. Li, Ultra-high-voltage Ni-rich layered cathodes in practical Li metal batteries enabled by a sulfonamide-based electrolyte, *Nat. Energy* 6 (2021) 495–505.
- [53] J. Zhang, H. Zhang, R. Li, L. Lv, D. Lu, S. Zhang, X. Xiao, S. Geng, F. Wang, T. Deng, L. Chen, X. Fan, Diluent decomposition-assisted formation of LiF -rich solid-electrolyte interfaces enables high-energy Li-metal batteries, *J. Energy Chem.* 78 (2023) 71–79.
- [54] S. Yu, Y. Zou, Q. Wang, J. Xu, C. Xiang, F. Xu, L. Sun, F. Yang, Self-supported Co-Mo sulfide in electrospun carbon nanofibers as electrocatalysts for hydrogen evolution reaction in alkaline medium, *J. Alloys Compd.* 911 (2022).
- [55] R. Han, Z. Wang, D. Huang, F. Zhang, A. Pan, H. Song, Y. Wei, Y. Liu, L. Wang, Y. Li, J. Xu, J. Hu, X. Wu, High-energy-density lithium metal batteries with impressive Li^+ transport dynamic and wide-temperature performance from -60 to 60°C , *Small* 19 (2023).



Yuxin Rao received a bachelor's degree from Jiangxi University of Science and Technology in 2021 and is currently pursuing a master's degree in the School of Physics and Materials Science at Nanchang University. His research mainly focuses on the preparation and modification of organic electrolytes for use in lithium metal batteries.



Xiang Liu obtained his bachelor's degree from Nanjing University of Science and Technology in 2012. In 2018, he completed his doctoral studies at Xiamen University. Then he joined BYD Co., Ltd as an engineer, engaged in silicon-based anodes research. In 2021, entering the School of Physics and Materials Science at Nanchang University, specializing in designing high-energy density lithium-ion battery materials, including cathodes, anodes, and pre-lithiation technology.



Xue Li received her bachelor's degree from Southwest University of Science and Technology in 2022, and is now pursuing her master's degree in the School of Physics and Materials Science at Nanchang University. Her main research interests are the optimization of functional electrolyte and anode interface stability for lithium metal batteries.



Naigen Zhou is Professor at Nanchang University, leading academic and technical figure in Jiangxi Province (leading talent) nominee. He worked as postdoctoral research at Brown University in the United States in 2008–2009. His main research involves computational simulation and experimental studies on new energy materials and devices for lithium batteries. Currently, he is the leader of the sub-discipline of new energy materials and devices in the "first-class discipline" of materials science and engineering at Nanchang University, as well as the leader of the energy materials and devices team at the School of Physics and Materials Science at Nanchang University.



Shangquan Zhao obtained his bachelor's degree from Xi'an Jiaotong University in 2014. He then went on to earn a master's degree from the China Academy of Engineering Physics in 2017. In 2021, he completed his doctoral studies at Xiamen University. After graduating, he joined the School of Physics and Materials Science at Nanchang University, where he specializes in first-principles calculations of lithium-ion battery materials, including cathodes, anodes, and electrolytes.



Shan Fang is an associate Professor at the School of Physics and Materials Science of Nanchang University. She received her Ph.D. at Nanjing University of Aeronautics and Astronautics (NCAA) in 2018, then worked as a staff scientist at Karlsruhe Institute of Technology (KIT), Helmholtz Institute Ulm (HIU) from 2018–2020. Her research interest is focusing on the high energy density anode and cathode materials for advanced lithium batteries.



Pengfei Liu is currently a graduate student of School of Physics and Materials, Nanchang University. His research interests focus on the modification of ionic liquid electrolytes applied in high-energy density lithium metal batteries.



Stefano Passerini is Professor at the Chemistry Department of the Sapienza University of Rome and Distinguished Senior Fellow at Karlsruhe Institute of Technology. His research focuses on the basic understanding and development of materials for high-energy batteries and supercapacitors, with the goal to create sustainable energy storage systems from environmentally friendly and available materials and processes. He has been awarded the Research Award of the Electrochemical Society Battery Division, and nominated Fellow of the International Society of Electrochemistry (2016) and the Electrochemical Society Inc (2020). Since 2019 he is a member of the Leopoldina German Academy of Science



Fanglin Wu received his bachelor degree from Sichuan University in 2015 and master degree from Wuhan University of Technology in 2017. Later, he completed his Ph.D. degree in Karlsruhe Institute of Technology (KIT) under the supervision of Prof. Dr. Stefano Passerini, and continued working in KIT as post-doctoral researcher. Currently, he is working in Wuhan University of Technology, his research is focusing on synthesis and modification of high specific-energy lithium-rich/nickel-rich cathodes as well as the matched high-safety ionic liquid electrolytes or solid state electrolytes for high energy density lithium metal batteries.